



HAL
open science

Measuring vector field correlations using diffraction

Miguel Alonso, Katelynn Sharma, Gregory Costello, Esteban Vélez-Juárez,
Thomas Brown

► **To cite this version:**

Miguel Alonso, Katelynn Sharma, Gregory Costello, Esteban Vélez-Juárez, Thomas Brown. Measuring vector field correlations using diffraction. *Optics Express*, 2018, 26 (7), 10.1364/OE.26.008301 . hal-01790608

HAL Id: hal-01790608

<https://amu.hal.science/hal-01790608>

Submitted on 27 Sep 2018

HAL is a multi-disciplinary open access archive for the deposit and dissemination of scientific research documents, whether they are published or not. The documents may come from teaching and research institutions in France or abroad, or from public or private research centers.

L'archive ouverte pluridisciplinaire **HAL**, est destinée au dépôt et à la diffusion de documents scientifiques de niveau recherche, publiés ou non, émanant des établissements d'enseignement et de recherche français ou étrangers, des laboratoires publics ou privés.



Measuring vector field correlations using diffraction

KATELYNN A. SHARMA,^{1,2} GREGORY COSTELLO,³ ESTEBAN VÉLEZ-JUÁREZ,⁴ THOMAS G. BROWN,¹ AND MIGUEL A. ALONSO^{1,5,6,*}

¹The Institute of Optics, University of Rochester, 275 Hutchison Road, Rochester, NY 14627, USA

²Laboratory for Laser Energetics, University of Rochester, 250 East River Road, Rochester, NY 14623, USA

³Physics and Astronomy Department, Stonehill College, 320 Washington Street, Easton, MA 02357, USA

⁴Facultad de Ciencias Físico Matemáticas, Benemérita Universidad Autónoma de Puebla, Puebla 72000, Mexico

⁵Center for Coherence and Quantum Optics, University of Rochester, Rochester, NY 14627, USA

⁶Aix-Marseille Univ., CNRS, Centrale Marseille, Institut Fresnel, UMR 7249, 13397 Marseille Cedex 20, France

*alonso@optics.rochester.edu

Abstract: We present a method for efficiently measuring the 2×2 correlation matrix for paraxial partially coherent beams by using diffraction from small apertures and obstacles. Several representations for this matrix function of four spatial variables are discussed and illustrated with experimental results, including various alternative definitions of the spatial degree of coherence.

© 2018 Optical Society of America

OCIS codes: (030.1640) Coherence; (050.1940) Diffraction; (070.2580) Paraxial wave optics.

References and links

1. E. Wolf, *Introduction to the Theory of Coherence and Polarization of Light* (Cambridge University, 2007), pp. 174–197.
2. H. P. Jauch and K. M. Bales, “Reversing-wave-front interferometry of radiation from a diffusely illuminated phase grating,” *Opt. Lett.* **7**, 127–129 (1982).
3. C. Iaconis and I. A. Walmsley, “Direct measurement of the two-point field correlation function,” *Opt. Lett.* **21**, 1783–1785 (1996).
4. D. Mendlovic, G. Shabtay, A. W. Lohmann, and N. Konforti, “Display of spatial coherence,” *Opt. Lett.* **23**, 1084–1086 (1998).
5. D. L. Marks, R. A. Stack and D. J. Brady, “Three-Dimensional Coherence Imaging in the Fresnel Domain,” *Appt. Opt.* **38**, 1332–1342 (1999).
6. C. C. Cheng, M. G. Raymer and H. Heier, “A variable lateral-shearing sagnac interferometer with high numerical aperture for measuring the complex spatial coherence of light,” *J. Mod. Opt.* **47**, 1237–1246 (2000).
7. G. A. Swartzlander Jr., R. I. Hernandez-Aranda, “Optical Rankine vortex and anomalous circulation of light,” *Phys. Rev. Lett.* **99**, 163901 (2007).
8. J. K. Wood, K. A. Sharma, S. Cho, T. G. Brown, and M. A. Alonso, “Using shadows to measure spatial coherence,” *Opt. Lett.* **39**, 4927–4930 (2014).
9. K. A. Sharma, T. G. Brown, and M. A. Alonso, “Phase-space approach to lensless measurements of optical field correlations,” *Opt. Express* **24**, 16099–16110 (2016).
10. E. Wolf, “Unified theory of coherence and polarization of random electromagnetic fields,” *Phys. Lett. A* **312**, 263–267 (2003).
11. S. A. Ponomarenko and E. Wolf, “The spectral degree of coherence of fully spatially coherent electromagnetic beams,” *Opt. Commun.* **227**, 73–74 (2003).
12. J. Tervo, S. Tero, and A. T. Friberg, “Degree of coherence for electromagnetic fields,” *Opt. Express* **11**, 1137–1143 (2003).
13. P. Réfrégier and A. Roueff, “Coherence polarization filtering and relation with intrinsic degrees of coherence,” *Opt. Lett.* **31**, 1175–1177 (2006).
14. F. Gori, M. Santarsiero and R. Borghi, “Maximizing Young’s fringe visibility through reversible optical transformations,” *Opt. Lett.* **32**, 588–590 (2007).
15. A. Luis, “Degree of coherence for vectorial electromagnetic fields as the distance between correlation matrices,” *J. Opt. Soc. Am. A* **24**, 1063–1068 (2007).
16. F. Zernike, “The concept of degree of coherence and its applications to optical problems,” *Physica* **5**, 785–795 (1938).
17. A. M. Beckley, T. G. Brown, and M. A. Alonso, “Full Poincaré beams,” *Opt. Express* **18**, 10777–10785 (2010).

18. T. G. Brown and A. M. Beckley, "Stress engineering and the applications of inhomogeneously polarized optical fields," *Frontiers of Optoelectronics* **6**, 89–96 (2013).
19. D. P. Brown and T. G. Brown, "Partially correlated azimuthal vortex illumination: Coherence and correlation measurements and effects in imaging," *Opt. Express* **281**, 20418–20426 (2008).
20. D. P. Brown and T. G. Brown, "Coherence measurements applied to critical and Köhler vortex illumination," *Proc. SPIE* **7184**, 71840B (2009).
21. M. Santarsiero and R. Borghi, "Measuring spatial coherence by using a reversed-wavefront Young interferometer," *Opt. Lett.* **31**, 861–863 (2006).

1. Introduction

The theory of spatial coherence provides a framework for modeling the propagation of statistically stationary partially coherent light [1]. In the case of quasimonochromatic light, the basic function in this theory is the mutual intensity, which provides the statistical correlation of the field at any pair of points. When the field is paraxial and its polarization is uniform, the vector character of light can be ignored and a scalar treatment suffices. However, in some cases the vector character of the electromagnetic field cannot be ignored and must be incorporated into the mutual intensity. For example, for paraxial beams, the mutual intensity is a 2×2 matrix composed of correlations between all transverse components of the electric field at two points \mathbf{x}_1 and \mathbf{x}_2 [1]:

$$\mathbb{J}(\mathbf{x}_1, \mathbf{x}_2) = \begin{bmatrix} J_{xx}(\mathbf{x}_1, \mathbf{x}_2) & J_{xy}(\mathbf{x}_1, \mathbf{x}_2) \\ J_{yx}(\mathbf{x}_1, \mathbf{x}_2) & J_{yy}(\mathbf{x}_1, \mathbf{x}_2) \end{bmatrix} = \begin{bmatrix} \langle E_x^*(\mathbf{x}_1)E_x(\mathbf{x}_2) \rangle & \langle E_x^*(\mathbf{x}_1)E_y(\mathbf{x}_2) \rangle \\ \langle E_y^*(\mathbf{x}_1)E_x(\mathbf{x}_2) \rangle & \langle E_y^*(\mathbf{x}_1)E_y(\mathbf{x}_2) \rangle \end{bmatrix}, \quad (1)$$

where E_x, E_y are the Cartesian components of the electric field, and the angular brackets denote a statistical correlation, corresponding to a temporal averaging performed by the detector. A full characterization of the beam requires the knowledge of all four complex elements of this matrix for all values of each of $\mathbf{x}_1 = (x_1, y_1)$ and $\mathbf{x}_2 = (x_2, y_2)$ over a transverse test plane. From this information, the propagation of the beam away from this plane can be modeled. Of course, in practice it is impossible to retrieve the mutual intensity matrix over all four spatial coordinates, and the best one can do is measure accurate estimates at a sufficiently dense sample of points within the region of the transverse plane where the beam is most significant. This task is simplified if the measurement technique provides simultaneously the mutual intensity for a large number of pairs of points. Several methods have been proposed to do this, based on the interferometric superposition of two copies of the wavefront [2–7].

Recently, a simple method for efficiently measuring the mutual intensity by using light diffraction around a small obstacle was proposed and demonstrated [8]. This approach has two attractive features. The first is that it provides simultaneous estimates for the field correlations at a large number of pairs of points, namely all pairs of points whose centroid is the centroid of the obstacle. The second is its simplicity, as it does not involve a complicated, vibration-sensitive interferometric setup in which the wavefront is separated and recombined. The only elements employed for the measurement are the obstacle (implemented with a spatial light modulator, or SLM), a lens to perform an optical Fourier transform, and a CCD detector. An extension of this approach was then proposed in which the lens is not required, even though this places some limitations in the range of validity of the method [9]. In this work we combine the advantages of the extended validity that results from using a lens [8] with the improvements that result from using not only diffraction from an obstacle but also from the complementary aperture [9]. In addition, we also incorporate polarization selection elements in order to allow measuring the complete matrix of correlations. This system is tested for fields with complex field correlations induced by an optical element with spatially varying birefringence. The resulting measurements are used to illustrate and compare with real data several proposed definitions of degree of coherence that incorporate the vector nature of light [10–15].

2. Descriptions for the spatial coherence of a paraxial electromagnetic beam over a transverse plane

As mentioned earlier, the mutual intensity matrix is a complex function over a large parameter space that includes four continuous spatial variables as well as two discrete polarization indices. This large dimensionality poses a problem not only for measurement but also for its graphic display and for the interpretation of the information it contains. For this reason, different alternative representations for this function have been proposed, in order to highlight different physical aspects of this large amount of information. We now give a brief summary of some of these representations.

Let us begin with the so-called generalized Stokes parameters [1], defined as

$$S_0(\mathbf{x}_1, \mathbf{x}_2) = \text{Tr}[\mathbb{J}(\mathbf{x}_1, \mathbf{x}_2)] = J_{xx}(\mathbf{x}_1, \mathbf{x}_2) + J_{yy}(\mathbf{x}_1, \mathbf{x}_2), \quad (2a)$$

$$S_1(\mathbf{x}_1, \mathbf{x}_2) = J_{xx}(\mathbf{x}_1, \mathbf{x}_2) - J_{yy}(\mathbf{x}_1, \mathbf{x}_2), \quad (2b)$$

$$S_2(\mathbf{x}_1, \mathbf{x}_2) = J_{pp}(\mathbf{x}_1, \mathbf{x}_2) - J_{mm}(\mathbf{x}_1, \mathbf{x}_2) = J_{xy}(\mathbf{x}_1, \mathbf{x}_2) + J_{yx}(\mathbf{x}_1, \mathbf{x}_2), \quad (2c)$$

$$S_3(\mathbf{x}_1, \mathbf{x}_2) = J_{rr}(\mathbf{x}_1, \mathbf{x}_2) - J_{ll}(\mathbf{x}_1, \mathbf{x}_2) = i [J_{xy}(\mathbf{x}_1, \mathbf{x}_2) - J_{yx}(\mathbf{x}_1, \mathbf{x}_2)], \quad (2d)$$

where the subindices p, m represent, respectively, field components along axes at $+45^\circ$ and -45° with respect to the x axis, and the subindices r, l indicate right- and left-hand circular components. The generalized Stokes parameters are defined as an extension of the standard Stokes parameters used in the study of polarization, and like these they are naturally related to simple measurements using polarization analyzers: each of the last three parameters corresponds to the difference of two measurements for two mutually orthogonal polarization components. Notice that in the limit when the two points \mathbf{x}_1 and \mathbf{x}_2 coincide, the generalized Stokes parameters reduce to the standard Stokes parameters for the corresponding point. The mutual intensity matrix can be written in terms of the generalized Stokes parameters as

$$\mathbb{J}(\mathbf{x}_1, \mathbf{x}_2) = \frac{1}{2} \begin{bmatrix} S_0(\mathbf{x}_1, \mathbf{x}_2) + S_1(\mathbf{x}_1, \mathbf{x}_2) & S_2(\mathbf{x}_1, \mathbf{x}_2) - iS_3(\mathbf{x}_1, \mathbf{x}_2) \\ S_2(\mathbf{x}_1, \mathbf{x}_2) + iS_3(\mathbf{x}_1, \mathbf{x}_2) & S_0(\mathbf{x}_1, \mathbf{x}_2) - S_1(\mathbf{x}_1, \mathbf{x}_2) \end{bmatrix} = \sum_{n=0}^3 \frac{S_n(\mathbf{x}_1, \mathbf{x}_2)}{2} \sigma_n, \quad (3)$$

where σ_0 is the 2×2 identity matrix and σ_n for $n = 1, 2, 3$ are the Pauli matrices.

In scalar treatments of coherence theory, the level of coherence between two points is characterized by the *degree of coherence* [16], which is related to the visibility of the fringes created by the interference of the light coming from these two points, say, in a two-pinhole experiment. Mathematically, this degree of coherence is simply given by the mutual intensity for the two points normalized by the geometric mean of the intensities at these two points. When the vector character of light is taken into account, however, the definition of the degree of coherence is not unique, as it depends on what aspect of the correlation between the two points is being considered. In this work we consider different sets of definitions that have been proposed in recent years, summarized in what follows.

The first definition is that by Wolf *et al.* [1, 10, 11], proposed as a direct extension of Zernike's degree of coherence for a scalar field in a two-pinhole experiment [16]: its magnitude equals the visibility of the fringes if the intensity at both pinholes is equal. Because a two-pinhole interference measurement would not reveal correlations between orthogonal components of the field, this definition involves only the diagonal elements of the mutual intensity matrix:

$$\mu_W(\mathbf{x}_1, \mathbf{x}_2) = \frac{\text{Tr}[\mathbb{J}(\mathbf{x}_1, \mathbf{x}_2)]}{\sqrt{\text{Tr}[\mathbb{J}(\mathbf{x}_1, \mathbf{x}_1)] \text{Tr}[\mathbb{J}(\mathbf{x}_2, \mathbf{x}_2)]}} = \frac{S_0(\mathbf{x}_1, \mathbf{x}_2)}{\sqrt{S_0(\mathbf{x}_1)S_0(\mathbf{x}_2)}}, \quad (4)$$

where $S_0(\mathbf{x}) = S_0(\mathbf{x}, \mathbf{x})$ is the total field intensity at \mathbf{x} .

The second definition was proposed by Tervo *et al.* [12], with the goal of providing a measure that also accounts for correlations between orthogonal components, and that is explicitly invariant

to unitary transformations of the field at each of the points. This definition can be expressed as

$$\mu_T(\mathbf{x}_1, \mathbf{x}_2) = \frac{\sqrt{\text{Tr}[\mathbb{J}(\mathbf{x}_1, \mathbf{x}_2)\mathbb{J}(\mathbf{x}_2, \mathbf{x}_1)]}}{\sqrt{\text{Tr}[\mathbb{J}(\mathbf{x}_1, \mathbf{x}_1)]\text{Tr}[\mathbb{J}(\mathbf{x}_2, \mathbf{x}_2)]}} = \frac{\sqrt{\sum_{n=0}^3 |S_n(\mathbf{x}_1, \mathbf{x}_2)|^2}}{\sqrt{2S_0(\mathbf{x}_1)S_0(\mathbf{x}_2)}}. \quad (5)$$

Note that, unlike the previous measure, μ_T does not necessarily equal unity when both its arguments coincide, since two different components of the field may be only partially correlated even at the same point. In this limit, this measure gives an expression related to the degree of polarization $P(\mathbf{x}) = \sqrt{2\text{Tr}[\mathbb{J}^2(\mathbf{x}, \mathbf{x})]/S_0^2(\mathbf{x})} - 1$ as $\mu_T(\mathbf{x}, \mathbf{x}) = \sqrt{[1 + P^2(\mathbf{x})]/2}$.

The third definition is due to Réfrégier and Roueff [13] and it actually provides two different measures, referred to by the authors as the intrinsic degrees of coherence, corresponding to

$$\mu_R^{(1,2)}(\mathbf{x}_1, \mathbf{x}_2) = \text{SV}_{1,2} \left[\mathbb{J}(\mathbf{x}_1, \mathbf{x}_1)^{-1/2} \mathbb{J}(\mathbf{x}_1, \mathbf{x}_2) \mathbb{J}(\mathbf{x}_2, \mathbf{x}_2)^{-1/2} \right], \quad (6)$$

where $\text{SV}_{1,2}(\cdot)$ denotes the two singular values of the matrix in its argument, ordered from largest to smallest. In particular, $\mu_R^{(1)}$ has a physical interpretation: it corresponds to the largest possible fringe visibility that can be achieved in a two-pinhole experiment if one is allowed to modify independently the light following each pinhole by placing any sequence of passive, dichroic birefringent masks (which perform linear transformations on the local field that are not necessarily unitary). While both singular values can be chosen as real and non-negative without loss of generality, we will allow $\mu_R^{(2)}$ to be either positive or negative for convenience.

A fourth definition follows from the work of Gori *et al.* [14] based on an idea similar to that of Réfrégier and Roueff [13]. This degree of coherence corresponds to the largest possible fringe visibility that can be achieved in a two-pinhole experiment if one is allowed to modify independently the light following each pinhole by placing any sequence of passive, transparent birefringent masks (which perform linear unitary transformations on the local field). The expression for this degree of coherence is given by

$$\mu_G(\mathbf{x}_1, \mathbf{x}_2) = \frac{\sum_{i=1,2} |\text{SV}_i[\mathbb{J}(\mathbf{x}_1, \mathbf{x}_2)]|}{\sqrt{S_0(\mathbf{x}_1)S_0(\mathbf{x}_2)}}. \quad (7)$$

The fifth definition was proposed by Luis [15] as a measure of correlation of the four-vector consisting of the two sets of field components at the two points in question:

$$\mu_L(\mathbf{x}_1, \mathbf{x}_2) = \sqrt{\frac{4}{3} \left[\frac{\text{Tr}(\mathbb{M}^2)}{(\text{Tr}\mathbb{M})^2} - \frac{1}{4} \right]}, \quad \mathbb{M} = \begin{bmatrix} \mathbb{J}(\mathbf{x}_1, \mathbf{x}_1) & \mathbb{J}(\mathbf{x}_1, \mathbf{x}_2) \\ \mathbb{J}(\mathbf{x}_2, \mathbf{x}_1) & \mathbb{J}(\mathbf{x}_2, \mathbf{x}_2) \end{bmatrix}. \quad (8)$$

(Note that the definition in [15] is actually the square of μ_L but we use the current form for uniformity with the remaining definitions.) This quantity is unusual because it is invariant to unitary transformations not only of the field at each point (achievable through transparent birefringent elements in front of the pinholes) but of the four-vector mentioned earlier (that is, of the 4×4 matrix \mathbb{M}). This includes transformations that are not physically straightforward to implement, such as swapping the x -components of the fields for the two points while leaving the y components unchanged. By manipulating this expression, one can find that μ_L can be written in terms of only μ_T and the intensities and degrees of polarization at the two points:

$$\mu_L(\mathbf{x}_1, \mathbf{x}_2) = \left\{ 2 \frac{P^2(\mathbf{x}_1)S_0^2(\mathbf{x}_1) + P^2(\mathbf{x}_2)S_0^2(\mathbf{x}_2) + [4\mu_T^2(\mathbf{x}_1, \mathbf{x}_2) - 2]S_0(\mathbf{x}_1)S_0(\mathbf{x}_2)}{3[S_0(\mathbf{x}_1) + S_0(\mathbf{x}_2)]^2} + \frac{1}{3} \right\}^{1/2}. \quad (9)$$

Notice that, unlike the other definitions of degree of coherence so far, μ_L does not necessarily go to zero for point separations that are far larger than the coherence width of the field, since it places

on equal footing correlations between components within each position and correlations between components for the two positions. This can be seen by setting $\mu_T \rightarrow 0$ in Eq. (9). In particular, if the intensity at the two points is the same but there is no statistical correlation between the field at these two points, one finds the limit $\mu_L(\mathbf{x}_1, \mathbf{x}_2) \rightarrow \sqrt{[P^2(\mathbf{x}_1) + P^2(\mathbf{x}_2)]}/6$.

3. Coherence measurement for each component

We now describe how the spatial coherence associated with a particular field component is measured in our setup. The key is the capture of images at a plane that is Fourier-conjugate to the plane where the coherence of the field is to be tested, the Fourier transformation being performed by a lens of focal distance f used in $2f$ configuration. A field component is selected through a combination of waveplates and polarizers and then made to pass through a simple aperture mask at the test plane. Let us assume that we select a field component E_j , namely that we want to measure the correlation $J_{jj}(\mathbf{x}_1, \mathbf{x}_2)$. This correlation can be estimated simultaneously for all pairs of points \mathbf{x}_1 and \mathbf{x}_2 with a fixed centroid \mathbf{x}_0 by taking three images in the Fourier plane: one with a clear mask, one with a small opaque obstacle centered at \mathbf{x}_0 , and one with the complementary small aperture centered at \mathbf{x}_0 . Let the measured intensities for these three images be denoted by $I^{(j)}(\mathbf{p})$, $I_O^{(j)}(\mathbf{p}; \mathbf{x}_0)$, and $I_A^{(j)}(\mathbf{p}; \mathbf{x}_0)$, where \mathbf{p} is the coordinate at the detector plane. Under the assumption that the aperture and obstacle are small compared to the scale of change of coherence, it can be shown by following steps like those in [8, 9] that the mutual intensity component is approximately proportional to the Fourier transform of a linear combination of these three measurements:

$$J_{jj}\left(\mathbf{x}_0 - \frac{\mathbf{x}'}{2}, \mathbf{x}_0 + \frac{\mathbf{x}'}{2}\right) \propto \iint \left[I^{(j)}(\mathbf{p}) - I_O^{(j)}(\mathbf{p}; \mathbf{x}_0) + I_A^{(j)}(\mathbf{p}; \mathbf{x}_0) - I_D^{(j)}(\mathbf{p}) \right] \exp\left(i \frac{k}{f} \mathbf{p} \cdot \mathbf{x}'\right) dx dy, \quad (10)$$

where $I_D^{(j)}(\mathbf{p})$ is a fourth measurement in which the SLM is completely darkened. In theory this fourth measurement should equal zero, but in practice it is needed for background subtraction. From the measurement of these correlations for different centroids \mathbf{x}_0 and for different field components, one can recover the generalized Stokes parameters and from them the mutual intensity matrix. In theory one can use as little as four field components, but experimental error is reduced by using more, and the choice of the standard six components ($j = x, y, p, m, r, l$) makes the calculation of the generalized Stokes parameters particularly straightforward.

4. Experimental implementation

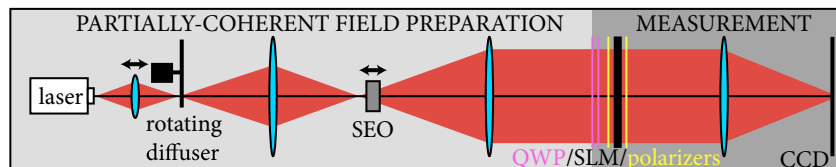


Fig. 1. Diagram of the experimental setup.

A diagram of the experimental setup is shown in Fig. 1. This setup is similar to that used in [8], but with important additions in order to introduce complex vector correlations as well as to measure them. The left part of the diagram describes the generation of the partially coherent field to be measured. A helium-neon laser ($\lambda = 633$ nm) is focused onto a rotating diffuser that preserves the degree of polarization of the incident beam. An image of this focus is formed with a lens, after which a second lens is used so that the field at the test plane is as collimated as possible.

The level of spatial coherence of the beam is controlled by changing the size of the focal spot at the diffuser, which is achieved by a longitudinal shift of the first lens. The intermediate image of this spot is used so that an optical element with spatially-varying birefringence can be inserted to generate nontrivial vector correlations. The element used here was a stress-engineered optic (SEO), [17, 18] which is a BK7 glass window subject to stress with trigonal symmetry, producing an interesting non-uniform birefringent distribution in which the retardance is proportional to the distance from the SEO's center and the orientation of the fast axis rotates as $-1/2$ times the azimuthal angle. In our measurements the beam was made to illuminate only the central part of the SEO, where the retardance reaches only up to a couple of waves. The SEO can be shifted longitudinally away from the focus to make the correlations at the test plane spatially inhomogeneous (that is, dependent on the centroid \mathbf{x}_0 of the two points).

The right part of the diagram in Fig. 1 shows the measurement apparatus, which consists of a polarization selection system, a controllable binary aperture mask, a lens to perform an optical Fourier transform, and a CCD to detect the resulting intensity distribution. The polarization selection system consists of two quarter-wave plates (QWPs) and a polarizer. The polarizer is nominally horizontal, to within a small calibration to optimize the performance of the SLM that follows it, as explained later. The two QWPs can be rotated in order to select the desired six field components, according to the nominal directions in Table 1. Given the slight adjustment of the polarizer and the fact that in practice these wave plates do not have exactly their nominal retardance, these orientations were also fine-tuned by reversing the direction of light propagation (i.e., placing the light source to the right of the polarizer and SLM) and verifying with a ThorLabs polarimeter that the desired polarizations were generated. A second polarizer is placed after the SLM, perpendicular to the first, so that the combination of the two polarizers and the SLM acts as a controllable amplitude mask. The orientations of these two polarizers were adjusted to optimize extinction of the dark SLM pixels, which is essential for this type of measurement (particularly when displaying a small aperture). To perform this adjustment, a full-scale reference image was first taken with the SLM set to full transmission and while using the maximum possible laser power. The SLM was then set to display a dark mask, the camera exposure was increased by $100\times$ and the gain was increased by $50\times$. By adjusting the polarizers to maximize extinction, the ratio of the reference bright image and the dark image was approximately $20\times$, so the extinction ratio was approximately $100,000:1$, which was the limit of the combined dynamic range of the camera and the laser.

Table 1. Angles of the two QWPs used to select the desired field components.

Field component	QWP 1	QWP 2
x	0°	0°
y	45°	45°
p	-22.5°	-22.5°
m	22.5°	22.5°
r	-45°	0°
l	45°	0°

5. Measurements

By selecting the appropriate positions of the QWPs, measurements were taken for the horizontal, vertical, $+45^\circ$, -45° , right-hand circular, and left-hand circular components. For each, images were captured with the mask open, with a square obstacle of side 1.56mm whose position was scanned over the test plane, with the complementary square aperture also scanned over the test plane, and with the SLM darkened. The corresponding components of the mutual intensity

were then calculated using Eq. (10). Figure 2(a) shows the corresponding components for the

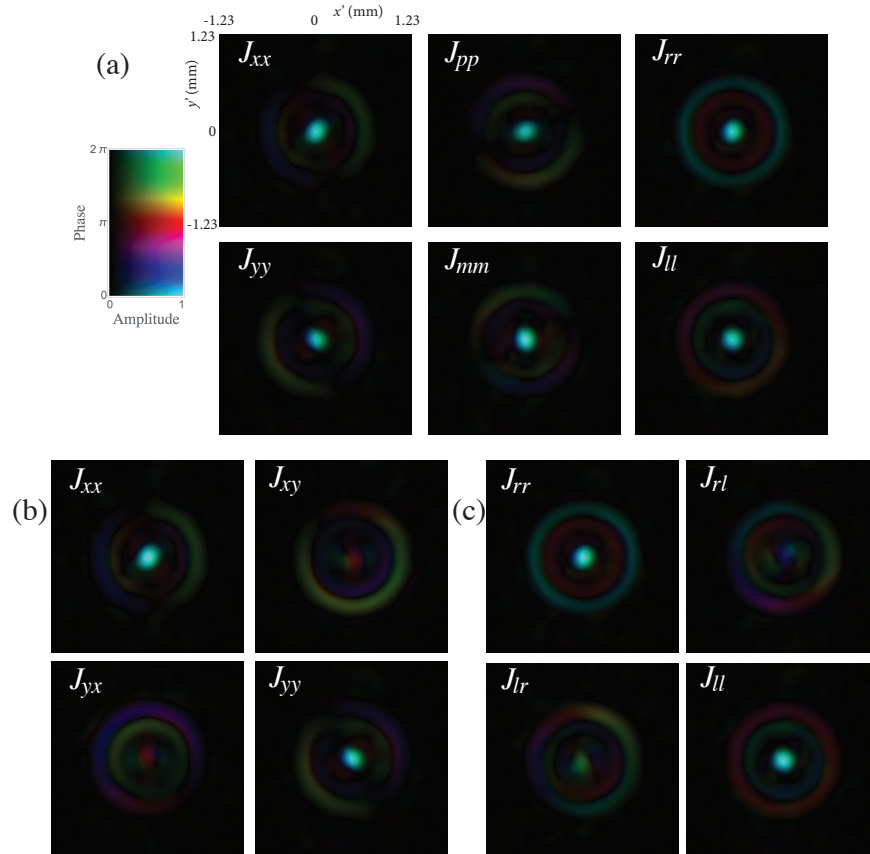


Fig. 2. (a) Measured components of the mutual intensity as a function of point separation (x' , y') for all pairs of points centered at the center of the test plane. The corresponding four components of the mutual intensity in the xy basis (b) and the rl basis (c).

case when the aperture/obstacle are at the center of the test plane. Notice that in this case the correlations are significant only for distances below the size of the aperture/obstacle used in the measurements. This is a feature of the scheme used here; the size of the aperture/obstacle places no upper or lower bound on the separation of the points over which the correlations can extend. What is important is that the aperture and obstacle are sufficiently small so that the mutual intensity (for fixed point separation) does not vary significantly as the point centroid varies within them [8].

From these measurements, one can calculate the four Cartesian components of \mathbb{J} by using Eqs. (2) and (3). These are shown in Fig. 2(b). For comparison, we also show in Fig. 2(c) the corresponding four components in the circular basis. We can see the interesting correlations created by placing the SEO at a Fourier-conjugate plane to the test plane; in particular, the correlation for the diagonal elements of the circular basis is essentially real and oscillates between positive and negative as a function of the point separation $|\mathbf{x}'|$.

We now use these measurements to compare the different definitions of the degree of coherence. For the fields we are measuring, the intensity $S_0(\mathbf{x})$ is roughly constant across the test plane, so we use the approximation $\sqrt{S_0(\mathbf{x}_1)S_0(\mathbf{x}_2)} \approx S_0(\mathbf{x}_0)$, where \mathbf{x}_0 is the centroid of \mathbf{x}_1 and \mathbf{x}_2 . Figure 3 shows side by side the results from these different definitions as functions of point separation

\mathbf{x}' for the same field as in Fig. 2(a). Note that, since μ_W is designed to ignore correlations between orthogonal components (introduced by the SEO in this case), it concentrates over short correlation distances. On the other hand, the remaining definitions, particularly $\mu_R^{(1)}$, highlight statistical correlations between more distant points, even if these correlations are over orthogonal components. The plots for μ_T and μ_G are mutually very similar except for small point separations, since the latter goes to unity as $\mathbf{x}' = \mathbf{0}$ while the former in this case only reaches a maximum value of 0.726. As mentioned earlier, μ_T and μ_L do not reduce to unity for $\mathbf{x}' = \mathbf{0}$ unless the field is fully polarized (which is not the case for this field). Also, note that unlike for the other definitions of degree of coherence, μ_L does not tend to zero for large point separations, since the field is not perfectly unpolarized.

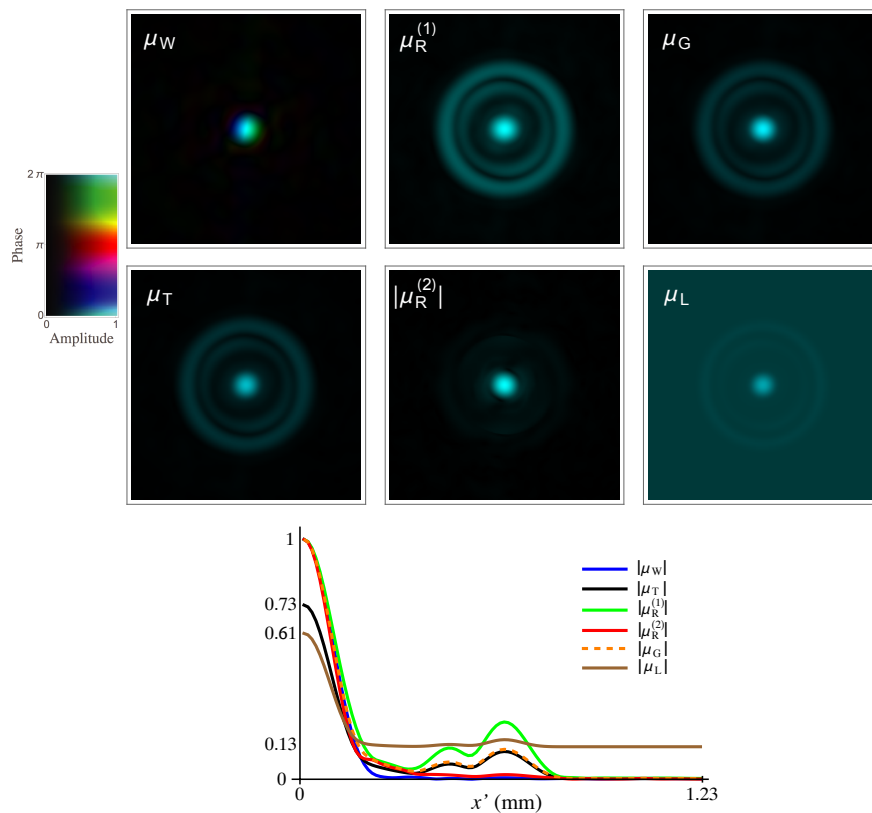


Fig. 3. Plots of the degree of coherence according to the six definitions discussed in this work, for the same field as in Fig. 2. The plot range and color palette is the same as in Fig. 2. The line plots at the bottom correspond to slices along the positive x' (horizontal) axis.

For comparison, Fig. 4 shows the corresponding results for a field where a larger section of the rotating diffuser is illuminated. In the scalar case (that is, for fields with uniform polarization), this would mean that the resulting field would have a shorter coherence width. However, notice that for fields with more complicated vector correlations we can only refer to the field in Fig. 4 as having significant shorter coherence width as that in Fig. 3 if we use μ_W (and perhaps $\mu_R^{(2)}$) as the criterion for defining coherence width. Otherwise, the range of point separations over which there are correlations is roughly the same for both fields, even though the features are more finely defined for the field in Fig. 4.

The plots shown so far are for the point centroid \mathbf{x}_0 fixed at the center of the test plane (namely,

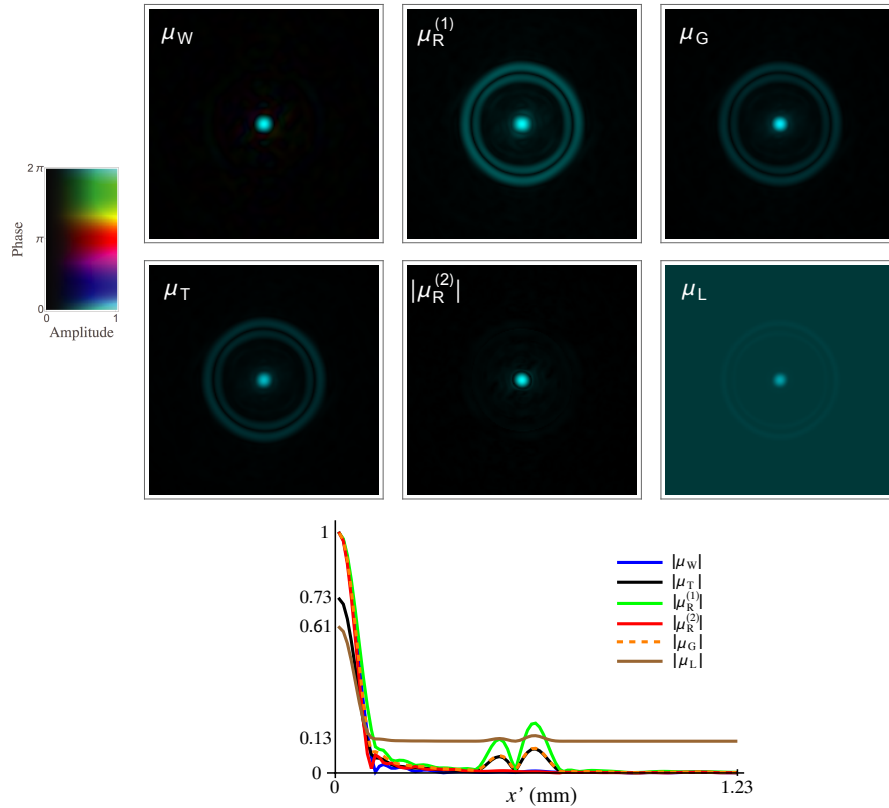


Fig. 4. Plots of the degree of coherence according to the six definitions discussed in this work, for a field generated by illuminating a larger spot at the diffuser as for the field in Figs. 2 and 3. The plot range and color palette is the same as in Fig. 2. The line plots at the bottom correspond to slices along the positive x' (horizontal) axis.

the center of the SLM). However, the mutual intensity is a function of four spatial variables, so in general it depends not only on the point separation \mathbf{x}' but also on \mathbf{x}_0 . By scanning the centroid of the aperture/obstacle over the test plane, one can sample the behavior of the mutual intensity over pairs of points with different centroids. Some of the corresponding measurements are shown in Fig. 5 for the case where the SEO was fixed at the intermediate image of the rotating diffuser, and in Fig. 6, where the SEO was shifted by 10 mm from this image plane in order to make the field less spatially homogeneous. For brevity we only show J_{II} . In these plots, the centroid \mathbf{x}_0 was scanned over a 5×5 array of points with spacing of 1.56 mm in both directions. [Visualization 1](#) and [Visualization 2](#) show how the different Cartesian components of \mathbb{J} and the six measures of the degree of coherence vary in these two cases. Notice that the individual components of \mathbb{J} change significantly with \mathbf{x}_0 , but that these changes are mostly in phase and not in magnitude. When the SEO is placed at the intermediate image of the diffuser ([Visualization 1](#)), the varying phase distribution is appreciably smoother than when the SEO is shifted ([Visualization 2](#)). Note also that the shapes of the degrees of coherence μ_W , μ_T and $\mu_R^{(1)}$ are fairly uniform in [Visualization 1](#), that is, they are approximately independent of centroid position, with the exception of some points towards the left margin where the variations in the coherence are probably due to a vignetting effect. The changes in these measures become more pronounced when the SEO is placed away from the intermediate focus ([Visualization 2](#)), since this displacement introduces space variance

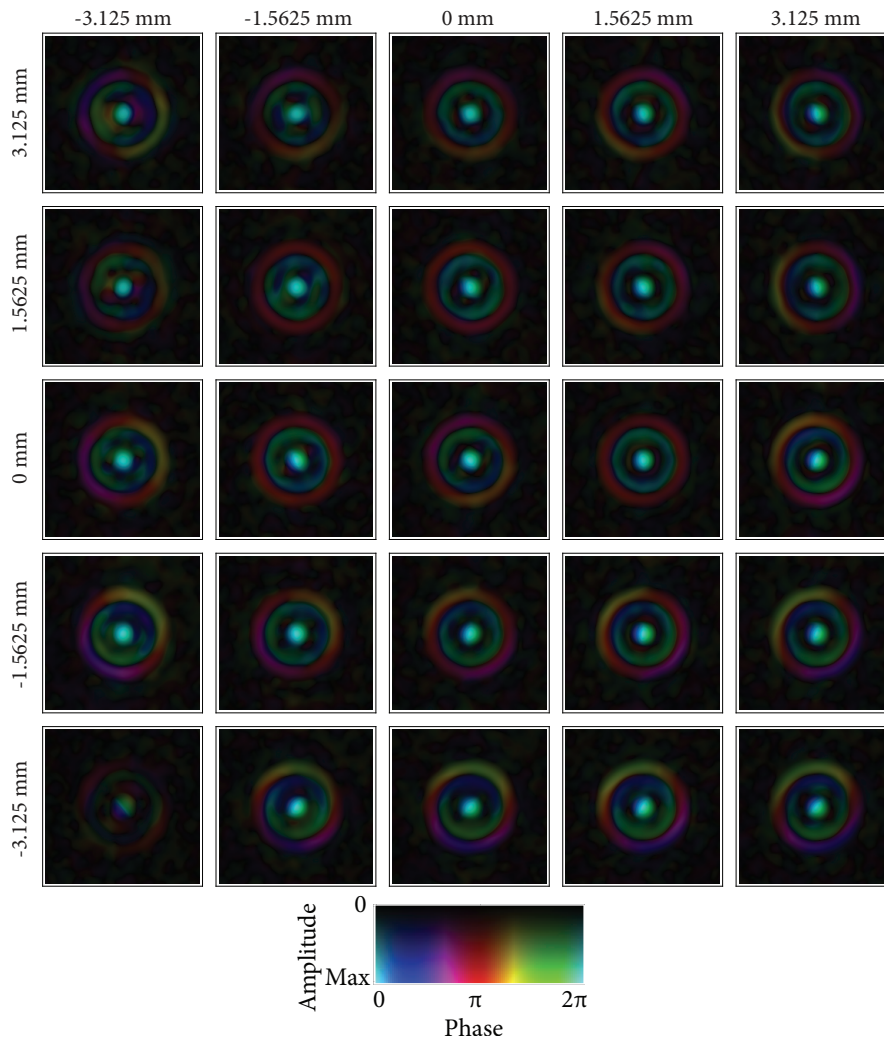


Fig. 5. J_{II} as a function of x' for a 5×5 array positions of the centroid \mathbf{x}_0 over the test plane with spacing of 1.56 mm, for a field generated with the SEO at the image plane of the rotating diffuser. [Visualization 1](#) shows for this sample of centroid points the corresponding variation of the four Cartesian components of the mutual intensity matrix and the degree of coherence according to the different definitions.

as the SEO is no longer centered at a plane that Fourier-conjugate to the test plane. Finally, note in both cases that the measures $\mu_R^{(2)}$ and μ_L fluctuate considerably, indicating that they are more sensitive to small changes in the field as well as to measurement or numeric errors. In the case of μ_L this change is mostly caused by the dependence of its background on the local degree of polarization.

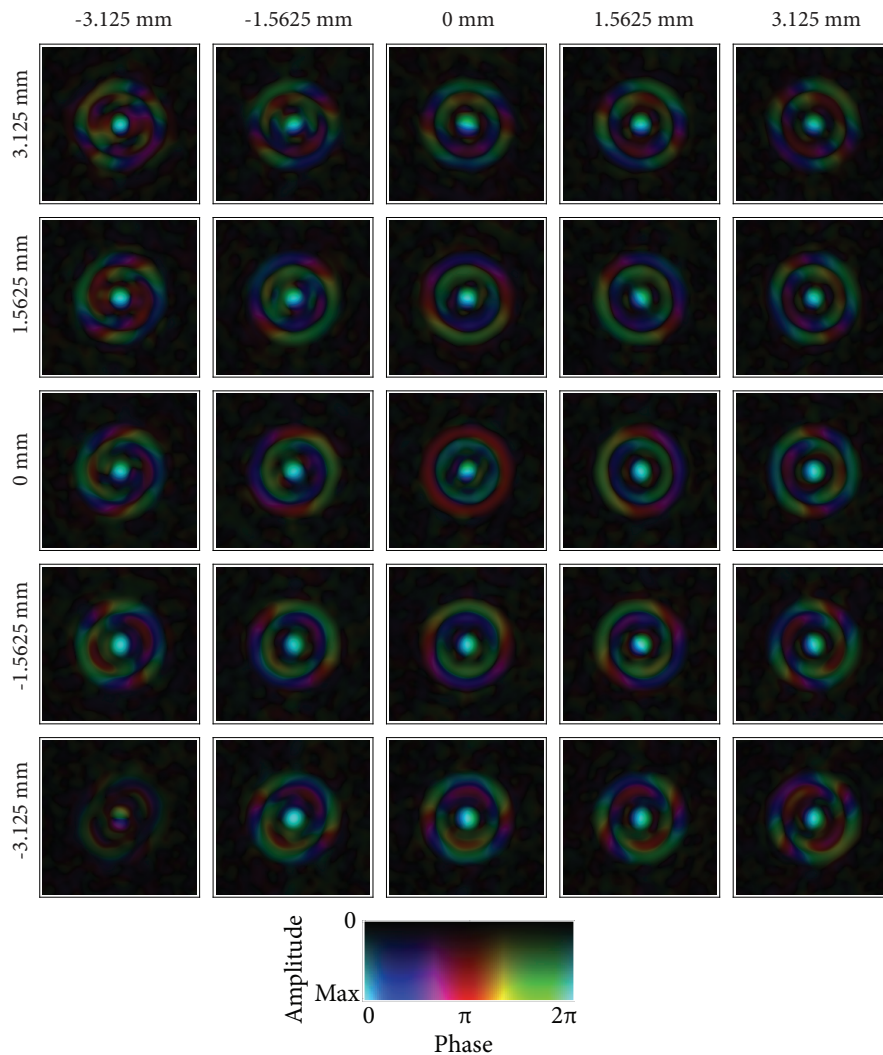


Fig. 6. J_{II} as a function of \mathbf{x}' for a 5×5 array positions of the centroid \mathbf{x}_0 over the test plane with spacing of 1.56 mm, for a field generated with the SEO at 10 mm from the image of the rotating diffuser. [Visualization 2](#) shows for this sample of centroid points the variation of the four Cartesian components of the mutual intensity matrix and the degree of coherence according to the different definitions.

6. Azimuthal illumination

Finally, we apply our setup to measure the mutual intensity matrix corresponding to a system with critical illumination composed of uncorrelated azimuthally polarized vortices. This type of illumination was proposed by Brown and Brown [19] as a way to enhance edge resolution in imaging systems, and was later shown to be equivalent to the corresponding Kohler illumination [20]. By design, the mutual intensity for this illumination is essentially spatially homogeneous, that is, it depends only on the vector separation \mathbf{x}' between the test points and not on their centroid

\mathbf{x}_0 . The following simple theoretical model was found for this field [19]:

$$\mathbb{J}\left(\mathbf{x}_0 - \frac{\mathbf{x}'}{2}, \mathbf{x}_0 + \frac{\mathbf{x}'}{2}\right) \propto w^{-2} \begin{bmatrix} w^2 - 2y'^2 & 2x'y' \\ 2x'y' & w^2 - 2x'^2 \end{bmatrix} \exp\left(-\frac{x'^2 + y'^2}{w^2}\right), \quad (11)$$

where w is a measure of the spatial coherence width. Note that for this simple model all the definitions of degree of coherence have a simple closed form:

$$\mu_W = (1 - \rho^2) \exp(-\rho^2), \quad (12a)$$

$$\mu_T = \sqrt{\frac{1 - 2\rho^2 + 2\rho^4}{2}} \exp(-\rho^2), \quad (12b)$$

$$\mu_R^{(1)} = \exp(-\rho^2), \quad (12c)$$

$$\mu_R^{(2)} = (1 - 2\rho^2) \exp(-\rho^2), \quad (12d)$$

$$\mu_G = \frac{1 + |1 - 2\rho^2|}{2} \exp(-\rho^2), \quad (12e)$$

$$\mu_L = \sqrt{\frac{1 - 2\rho^2 + 2\rho^4}{3}} \exp(-\rho^2), \quad (12f)$$

where $\rho = |\mathbf{x}'|/w$. These functions are plotted in Fig. 7. Note that neither μ_T nor μ_L equal unity as $\rho \rightarrow 0$ because the field is actually fully unpolarized at all points (but $\mu_L \rightarrow 0$ for large ρ for the same reason). In fact, these two measures differ only by a numerical factor in this case. Also, μ_W happens to be the average of the two intrinsic degrees of coherence $\mu_R^{(1,2)}$ if the sign of $\mu_R^{(2)}$ is chosen so that it is a smooth function, while μ_G is the average of these two intrinsic degrees of coherence if $\mu_R^{(2)}$ is chosen as non-negative. That is, $\mu_W = \mu_G$ up to the zero of $\mu_R^{(2)}$.

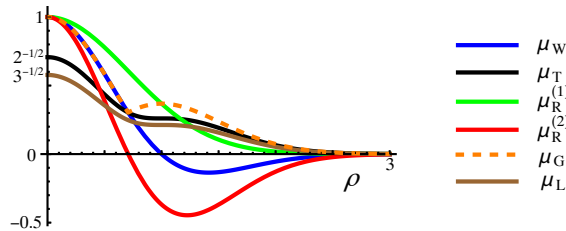


Fig. 7. Plots of the expressions in Eqs. (12) for the six definitions of degree of coherence as functions of the scaled point separation $\rho = |\mathbf{x}'|/w$ for the theoretical model of azimuthal illumination.

In [19], this illumination was experimentally implemented and its mutual intensity measured for a few pairs of points using a reversed-wavefront Young two-pinhole interferometer [21], requiring a measurement for each point pair. The setup presented in this work, on the other hand, allows recovering the complete matrix for a large set of point separations based on only four measurements per component. The desired field was generated by placing at the image of the diffuser a SEO in which only the central part (where the retardance is below one wave) was illuminated, in order to create the appropriate vortex correlations, followed by an azimuthal polarizer to select the appropriate polarization components. The resulting measurements are shown to agree well with the theoretical model in Eq. (11) in Fig. 8.

7. Concluding remarks

A simple optical setup was shown to be able to measure efficiently all components of the mutual intensity matrix over a large number of pairs of sample points. The method was tested with

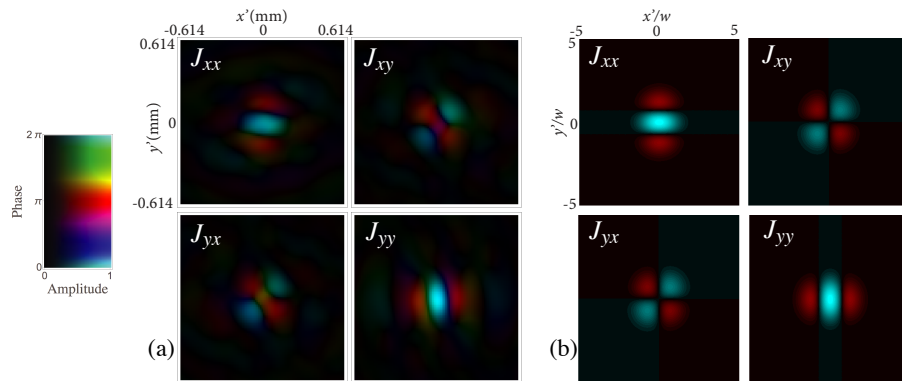


Fig. 8. (a) Measured and (b) theoretical components of the mutual intensity matrix in terms of point separation, for critical illumination with azimuthal vortex correlations, following Eq. (11). The color scheme is the same as in previous images, but because the correlations are essentially real, only positive (aqua) and negative (red) values are appreciable.

partially coherent fields generated by using a rotating diffuser as well as an optical element with an inhomogeneous birefringence distribution to create nontrivial correlations between components. The measurement results were used to illustrate several different definitions of degree of coherence for electromagnetic beams, highlighting the different aspects of the field correlations that each of these definition seeks to emphasize. The setup was also used to measure and compare with theory a field with azimuthal vortex correlation.

Funding

National Science Foundation (NSF) (PHY-1507278). GC was funded through a REU supplement to this award. KAS was funded through a Horton Fellowship from the Laboratory for Laser Energetics. EVJ was funded through a CONACYT *Beca Mixta* Fellowship. MAA received funding from the Excellence Initiative of Aix-Marseille University - A*MIDEX, a French “Investissements d’Avenir” programme.

Acknowledgments

We thank Anthony Vella and Ashan Ariyawansa for help with computational procedures and the experimental setup, and Massimo Santarsiero and Philippe Réfrégier for useful discussions.